ELSEVIER

Composites: Part B 31 (2000) 97–106

composites
Part B: engineering

www.elsevier.com/locate/compositesb

# Three-dimensional thermoelastic deformations of a functionally graded elliptic plate

Z.-Q. Cheng[a], R.C. Batra[b,*]

[a]Department of Modern Mechanics, University of Science and Technology of China, Hefei, Anhui 230026, People's Republic of China
[b]Department of Engineering Science and Mechanics, Virginia Polytechnic Institute and State University, Blacksburg, VA 24061-0219, USA

Received 24 February 1999; accepted 4 October 1999

**Abstract**

A new solution in closed form is obtained for the thermomechanical deformations of an isotropic linear thermoelastic functionally graded elliptic plate rigidly clamped at the edges. The through-thickness variation of the volume fraction of the ceramic phase in a metal–ceramic plate is assumed to be given by a power-law type function. The effective material properties at a point are computed by the Mori–Tanaka scheme. It is found that the through-thickness distributions of the in-plane displacements and transverse shear stresses in a functionally graded plate do not agree with those assumed in classical and shear deformation plate theories. © 2000 Elsevier Science Ltd. All rights reserved.

*Keywords*: Thermomechanical deformations; C. Analytical modeling

## 1. Introduction

Macroscopically inhomogeneous materials commonly appear in all kinds of engineering structures [1,2]. For example in laminated structures, material properties are piecewise constant in the thickness direction. A sudden change in material properties at the interfaces can result in locally large plastic deformations which may trigger the initiation and propagation of a micro-crack or even a fatal crack in a lamina. These adverse interface effects are mitigated in a new class of materials termed "functionally gradient materials". Functionally gradient materials are spatial composites in which material properties vary continuously. This is achieved by gradually changing the volume fraction of the constituent materials usually in one (the thickness) direction to obtain a smooth variation of material properties and an optimum response to external thermomechanical loads. These materials are being used in aerospace and power generation industries [3].

There are several two- (2D) and three-dimensional (3D) theories available to analyze the thermoelastic deformations of inhomogeneous structures. However, most of these studies have been conducted for laminated structures. For structures made of functionally gradient materials, it is desirable to obtain closed form solutions from 3D theories to assess the accuracy and validity of 2D theories.

The method of asymptotic expansion [4–6] has been developed to analyze 3D deformations of inhomogeneous plates. In Ref. [4], however, material properties and the deformations of the plate have been assumed to be symmetric about the mid-plane of the elliptic plate. However, such is not the case in general for a functionally graded plate. In the other two studies [5,6] numerical examples are given only for rectangular laminated plates.

Here the method of asymptotic expansion has been used to study three-dimensional mechanical deformations of an isotropic linear thermoelastic elliptic plate, and the deformations due to thermal loads are straightforwardly found. The plate is made of a functionally graded material and has edges rigidly clamped at the mid-plane. The closed-form analytical solution of the problem reveals that the available plate theories are insufficient to describe the thermomechanical behavior of functionally graded plates. The present solution can also be used to assess the accuracy of different plate theories and other numerical techniques.

## 2. Formulation of the problem

We use rectangular Cartesian coordinates $x_i$, $i = 1, 2, 3$, with the plane $x_3 = 0$ coincident with the mid-plane of the elliptic plate, to describe its thermomechanical deformations.

* Corresponding author. Tel.: + 1-540-231-6051; fax: + 1-540-231-4574.
*E-mail address:* rbatra@vt.edu (R.C. Batra).


PII: S1359-8368(99)00069-4

As shown in Fig. 1, the plate is of thickness $h$ and its semi-major and semi-minor axes equal $a$ and $b$, respectively. We assume that the plate is made of an isotropic material with material properties varying smoothly in the $x_3$ (thickness) direction only. In the absence of body forces, equations of elastostatics that govern the deformations of the plate are

$$\partial_j \sigma_{ij} = 0, \qquad \epsilon_{ij} = \frac{1}{2}(\partial_j u_i + \partial_i u_j),$$
$$\sigma_{ij} = 2\mu\epsilon_{ij} + [\lambda\epsilon_{kk} - (3\lambda + 2\mu)\alpha T]\delta_{ij}, \tag{1}$$

where $\sigma_{ij}$ is the stress tensor, $\epsilon_{ij}$ the infinitesimal strain tensor, $u_i$ the displacement of a point, $T$ the change in temperature from that in the stress free reference configuration, $\partial_i \equiv \partial/\partial x_i$ and $\delta_{ij}$ is the Kronecker delta. A repeated index implies summation over the range of the index with Latin indices ranging from 1 to 3 and Greek indices from 1 to 2. The Lamé coefficients, $\lambda$ and $\mu$, and the coefficient of thermal expansion, $\alpha$, are functions of $x_3$.

Eq. (1) may be rewritten in the form of a transfer matrix as

$$\partial_3 \begin{bmatrix} \mathbf{F} \\ \mathbf{G} \end{bmatrix} = \begin{bmatrix} \mathbf{0} & \mathbf{A} \\ \mathbf{B} & \mathbf{0} \end{bmatrix} \begin{bmatrix} \mathbf{F} \\ \mathbf{G} \end{bmatrix} + \begin{bmatrix} \mathbf{0} \\ \mathbf{C} \end{bmatrix} T, \tag{2}$$

where

$$\mathbf{F} = \begin{bmatrix} u_1 \\ u_2 \\ \sigma_{33} \end{bmatrix}, \qquad \mathbf{G} = \begin{bmatrix} \sigma_{13} \\ \sigma_{23} \\ u_3 \end{bmatrix}, \tag{3}$$

$$\mathbf{A} = \begin{bmatrix} \frac{1}{\mu} & 0 & -\partial_1 \\ 0 & \frac{1}{\mu} & -\partial_2 \\ -\partial_1 & -\partial_2 & 0 \end{bmatrix}, \quad \mathbf{C} = k\alpha \begin{bmatrix} 2\mu\partial_1 \\ 2\mu\partial_2 \\ 1 \end{bmatrix}, \quad k = \frac{3\lambda + 2\mu}{\lambda + 2\mu},$$
$$\mathbf{B} = \begin{bmatrix} -\frac{4\mu(\lambda+\mu)}{\lambda+2\mu}\partial_1^2 - \mu\partial_2^2 & -\mu k\partial_1\partial_2 & -\frac{\lambda}{\lambda+2\mu}\partial_1 \\ -\mu k\partial_1\partial_2 & -\mu\partial_1^2 - \frac{4\mu(\lambda+\mu)}{\lambda+2\mu}\partial_2^2 & -\frac{\lambda}{\lambda+2\mu}\partial_2 \\ -\frac{\lambda}{\lambda+2\mu}\partial_1 & -\frac{\lambda}{\lambda+2\mu}\partial_2 & \frac{1}{\lambda+2\mu} \end{bmatrix}. \tag{4}$$

The longitudinal stresses are given by

$$\sigma_{\alpha\beta} = \frac{2\lambda\mu}{\lambda+2\mu}\partial_\omega u_\omega \delta_{\alpha\beta} + \mu(\partial_\beta u_\alpha + \partial_\alpha u_\beta) + \frac{\lambda}{\lambda+2\mu}\sigma_{33}\delta_{\alpha\beta} - 2\mu k\alpha T\delta_{\alpha\beta}. \tag{5}$$

As is usually done in two-dimensional plate theories, the mechanical boundary conditions at a rigidly clamped edge are approximated by

$$u_1 = u_2 = u_3 = 0, \qquad \frac{\partial u_3}{\partial n_0} = 0,$$
$$\text{at } \frac{x_1^2}{a^2} + \frac{x_2^2}{b^2} - 1 = 0 \qquad \text{and} \qquad x_3 = 0. \tag{6}$$

Here $\mathbf{n}_0$ denotes the outward unit normal to the edge of the elliptic plate. It should be noted that these conditions hold only at the mid-plane of the plate, thus boundary layer effects generally found in three-dimensional analysis of the problem are neglected. For the linear thermoelastic problem under consideration, deformations due to the combined thermomechanical loads can be ascertained by superposing the deformation due to thermal loads and that due to mechanical loads. Hence we separately study the two problems.

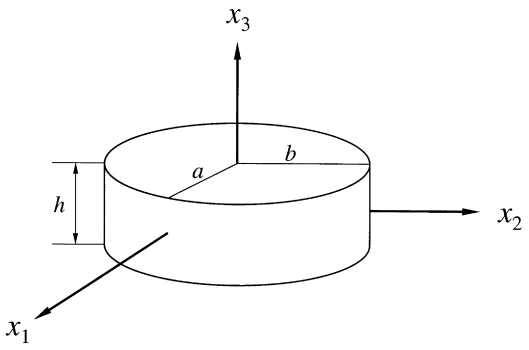


Fig. 1. Geometry of an elliptic plate.

## 3. Deformation due to thermal loads

It is assumed that steady-state conditions prevail and the temperature field in the plate is a function of $x_3$ only. The heat conduction equation and the thermal boundary conditions on

the top and bottom surfaces are

$$\partial_3(\kappa\partial_3 T) = 0, \qquad T\left(\pm\frac{h}{2}\right) = T^{\pm}, \tag{7}$$

where $\kappa$, the thermal conductivity coefficient, is a function of $x_3$, and $T^{\pm}$ are, respectively, the uniform ambient temperatures on the top and bottom surfaces of the plate. The solution of the boundary value problem (7) is

$$T(x_3) = T^{-} + (T^{+} - T^{-})\frac{\int_{-h/2}^{x_3}\frac{1}{\kappa}\,\mathrm{d}x_3}{\int_{-h/2}^{h/2}\frac{1}{\kappa}\,\mathrm{d}x_3}. \tag{8}$$

The deformations of the plate can now be calculated from Eq. (2) and boundary condition (6). The non-zero displacement and stresses are

$$u_3 = \int_0^{x_3} k\alpha T\,\mathrm{d}x_3, \qquad \sigma_{11} = \sigma_{22} = -2\mu k\alpha T. \tag{9}$$

As the transverse stresses vanish, the top and bottom surfaces of the plate are traction free. Eq. (9) implies that the plate expands or contracts in the thickness direction only, and because of the edges being clamped, it is subjected to in-plane tensions and/or compressions. The in-plane tensions and/or compressions vary only in the thickness direction. We note that the foregoing solution applies to a plate of an arbitrary shape. However, because the edge conditions are satisfied only on the mid-plane of the plate, this solution is not valid at points near the edges of the plate.

## 4. Deformation due to mechanical loads

Assume that tangential tractions, $q_\alpha^{\pm}$, and normal pressures, $q_3^{\pm}$, are applied on the top and bottom surfaces of the plate. An asymptotic expansion method is used to solve the problem. We introduce the small parameter $\epsilon = h/2a$ and scale the thickness coordinate by $x_3 = \epsilon z$; thus $z$ varies from $-a$ to $a$ as $x_3$ goes from $-h/2$ to $h/2$. The state space equation (2) can now be written as

$$\partial_z\begin{bmatrix}\mathbf{F}\\ \mathbf{G}\end{bmatrix} = \epsilon\begin{bmatrix}\mathbf{0} & \mathbf{A}\\ \mathbf{B} & \mathbf{0}\end{bmatrix}\begin{bmatrix}\mathbf{F}\\ \mathbf{G}\end{bmatrix}, \tag{10}$$

and its solution is

$$\begin{bmatrix}\mathbf{F}\\ \mathbf{G}\end{bmatrix} = \mathbf{P}\begin{bmatrix}\mathbf{F}(0)\\ \mathbf{G}(0)\end{bmatrix}, \tag{11}$$

where $\mathbf{P}$ is the transfer matrix which propagates the state space functions (3) from the reference plane $z = 0$ to a plane $z =$ constant. In terms of the integral operators

$$Q(\cdots) \equiv \int_0^z (\cdots)\mathrm{d}z, \qquad \bar{Q}(\cdots) \equiv \int_0^a (\cdots)\,\mathrm{d}z,$$
$$\hat{Q}(\cdots) \equiv \int_{-a}^{a} (\cdots)\,\mathrm{d}z, \tag{12}$$

the transfer matrix becomes

$$\mathbf{P} = \sum_{n=0}^{\infty}\epsilon^{2n}\begin{bmatrix}\mathbf{a}^{(2n)} & \epsilon\mathbf{a}^{(2n+1)}\\ \epsilon\mathbf{b}^{(2n+1)} & \mathbf{b}^{(2n)}\end{bmatrix}, \tag{13}$$

where

$$\mathbf{a}^{(n+1)} = Q\mathbf{A}\mathbf{b}^{(n)}, \quad \mathbf{b}^{(n+1)} = Q\mathbf{B}\mathbf{a}^{(n)}, \qquad (n \geq 0), \tag{14}$$

and

$$\mathbf{a}^{(0)} = \mathbf{b}^{(0)} = \mathbf{i} \tag{15}$$

is a $3\times 3$ identity matrix.

We expand the state space variables $\mathbf{F}$ and $\mathbf{G}$ in terms of the small parameter $\epsilon$ as

$$\begin{bmatrix}\mathbf{F}\\ \mathbf{G}\end{bmatrix} = \sum_{n=0}^{\infty}\epsilon^{2n}\begin{bmatrix}\epsilon\mathbf{f}^{(n)}\\ \mathbf{g}^{(n)}\end{bmatrix}, \tag{16}$$

and substitute it and Eq. (13) into Eq. (11) to obtain

$$\mathbf{f}^{(n)} = \sum_{k=0}^{n}\left[\mathbf{a}^{(2k)}\mathbf{f}^{(n-k)}(0) + \mathbf{a}^{(2k+1)}\mathbf{g}^{(n-k)}(0)\right], \quad (n \geq 0),$$
$$\mathbf{g}^{(0)} = \mathbf{g}^{(0)}(0), \tag{17}$$
$$\mathbf{g}^{(n)} = \sum_{k=0}^{n-1}\mathbf{b}^{(2k+1)}\mathbf{f}^{(n-1-k)}(0) + \sum_{k=0}^{n}\mathbf{b}^{(2k)}\mathbf{g}^{(n-k)}(0), \quad (n \geq 1).$$

For general mechanical loading conditions, excluding the particular case of equal and opposite tractions on the top and bottom surfaces, the transverse shear stresses are $O(\epsilon^2)$ and the transverse normal stress is $O(\epsilon^3)$. The surface conditions are then scaled by

$$\sigma_{13}(\pm a) = \epsilon^2 q_1^{\pm}, \qquad \sigma_{23}(\pm a) = \epsilon^2 q_2^{\pm},$$
$$\sigma_{33}(\pm a) = -\epsilon^3 q_3^{\pm}. \tag{18}$$

They can be further expressed, with the help of Eq. (16), by a hierarchy of formulations of orders 0–infinity, in which the load terms only appear in the following equations:

$$\sigma_{13}^{(1)}(0) + b_{1\omega}^{(1)}(\pm a)U_\omega^{(0)} + b_{13}^{(2)}(\pm a)U_3^{(0)} = q_1^{\pm},$$
$$\sigma_{23}^{(1)}(0) + b_{2\omega}^{(1)}(\pm a)U_\omega^{(0)} + b_{23}^{(2)}(\pm a)U_3^{(0)} = q_2^{\pm},$$
$$\sigma_{33}^{(1)}(0) + a_{3\alpha}^{(1)}(\pm a)\sigma_{\alpha 3}^{(1)}(0)$$
$$+a_{3\omega}^{(2)}(\pm a)U_\omega^{(0)} + a_{33}^{(3)}(\pm a)U_3^{(0)} = -q_3^{\pm}, \tag{19}$$

where

$$U_i^{(n)} \equiv u_i^{(n)}(x_\rho, 0). \tag{20}$$

Eliminating the transverse stresses from Eq. (19) and evaluating some relevant operators in terms of Eq. (14) we

obtain

$$\begin{bmatrix} -\hat{Q}\gamma\partial_1^2 - \hat{Q}\mu\partial_2^2 & -\hat{Q}(\gamma-\mu)\partial_1\partial_2 & \hat{Q}z\gamma\nabla^2\partial_1 \\ -\hat{Q}(\gamma-\mu)\partial_1\partial_2 & -\hat{Q}\mu\partial_1^2 - \hat{Q}\gamma\partial_2^2 & \hat{Q}z\gamma\nabla^2\partial_2 \\ -\hat{Q}z\gamma\nabla^2\partial_1 & -\hat{Q}z\gamma\nabla^2\partial_2 & \hat{Q}z^2\gamma\nabla^4 \end{bmatrix} \begin{bmatrix} U_1^{(0)} \\ U_2^{(0)} \\ U_3^{(0)} \end{bmatrix} = \begin{bmatrix} q_1^+ - q_1^- \\ q_2^+ - q_2^- \\ -(q_3^+ - q_3^-) + a\partial_\alpha(q_\alpha^+ + q_\alpha^-) \end{bmatrix}, \tag{21}$$

where

$$\nabla^2 = \partial_1^2 + \partial_2^2, \qquad \gamma = \frac{4\mu(\lambda+\mu)}{\lambda+2\mu}. \tag{22}$$

Eqs. (21) are the governing equations of the leading order for the functionally graded plate and are of the same form as those derived by using the two-dimensional classical Kirchhoff theory.

We now assume that the top and bottom surfaces of the plate are only subjected to uniform normal pressure $q_3^{\pm}$. To the leading order the edge conditions for the elliptic plate are

$$U_1^{(0)} = U_2^{(0)} = U_3^{(0)} = 0,$$
$$\frac{\partial U_3^{(0)}}{\partial n_0} = 0, \ \text{at} \ \frac{x_1^2}{a^2} + \frac{x_2^2}{b^2} - 1 = 0, \tag{23}$$

and the solution satisfying these conditions is

$$U_1^{(0)} = (q_3^+ - q_3^-)\frac{C}{a^2}x_1\left(\frac{x_1^2}{a^2} + \frac{x_2^2}{b^2} - 1\right),$$
$$U_2^{(0)} = (q_3^+ - q_3^-)\frac{C}{b^2}x_2\left(\frac{x_1^2}{a^2} + \frac{x_2^2}{b^2} - 1\right), \tag{24}$$
$$U_3^{(0)} = -(q_3^+ - q_3^-)\frac{D}{4}\left(\frac{x_1^2}{a^2} + \frac{x_2^2}{b^2} - 1\right)^2,$$

with

$$C = -\frac{\hat{Q}z\gamma}{\hat{Q}\gamma}D,$$
$$D^{-1} = 2\left(\frac{3}{a^4} + \frac{2}{a^2b^2} + \frac{3}{b^4}\right)\left[\hat{Q}z^2\gamma - \frac{(\hat{Q}z\gamma)^2}{\hat{Q}\gamma}\right]. \tag{25}$$

Eqs. (19) give

$$\sigma_{13}^{(1)}(0) = (q_3^+ - q_3^-)c_1x_1, \qquad \sigma_{23}^{(1)}(0) = (q_3^+ - q_3^-)c_2x_2,$$
$$\sigma_{33}^{(1)}(0) = -q_3^+ + (q_3^+ - q_3^-)c_3, \tag{26}$$

where

$$c_1 = \frac{2}{a^2}\left(\frac{3}{a^2} + \frac{1}{b^2}\right)\bar{Q}\gamma(C + Dz),$$
$$c_2 = \frac{2}{b^2}\left(\frac{1}{a^2} + \frac{3}{b^2}\right)\bar{Q}\gamma(C + Dz), \tag{27}$$
$$c_3 = 2\left(\frac{3}{a^4} + \frac{2}{a^2b^2} + \frac{3}{b^4}\right)\bar{Q}z\gamma(C + Dz).$$

The governing equations of higher-orders are obtained from Eqs. (16)–(18). Omitting details, we only note that all higher-order unknowns identically vanish. Therefore, the non-zero reference solution on the mid-plane is

$$\mathbf{f}^{(0)}(0) = \begin{bmatrix} U_1^{(0)} \\ U_2^{(0)} \\ 0 \end{bmatrix}, \qquad \mathbf{g}^{(0)}(0) = \begin{bmatrix} 0 \\ 0 \\ U_3^{(0)} \end{bmatrix},$$
$$\mathbf{f}^{(1)}(0) = \begin{bmatrix} 0 \\ 0 \\ \sigma_{33}^{(1)}(0) \end{bmatrix}, \qquad \mathbf{g}^{(1)}(0) = \begin{bmatrix} \sigma_{13}^{(1)}(0) \\ \sigma_{23}^{(1)}(0) \\ 0 \end{bmatrix}. \tag{28}$$

Any of the through-thickness displacements and stresses can be evaluated from the reference solution by straightforward differentiations with respect to $x_\alpha$ and integrations with respect to $z$ (or $x_3$). The complete through-thickness solution is obtained by substituting the reference solution (28) into Eq. (17), i.e.

$$\mathbf{g}^{(0)} = \mathbf{g}^{(0)}(0), \ \ \mathbf{f}^{(0)} = \mathbf{f}^{(0)}(0) + \mathbf{a}^{(1)}\mathbf{g}^{(0)}(0),$$
$$\mathbf{g}^{(1)} = \mathbf{g}^{(1)}(0) + \mathbf{b}^{(1)}\mathbf{f}^{(0)}(0) + \mathbf{b}^{(2)}\mathbf{g}^{(0)}(0), \tag{29}$$
$$\mathbf{f}^{(1)} = \mathbf{f}^{(1)}(0) + \mathbf{a}^{(1)}\mathbf{g}^{(1)}(0) + \mathbf{a}^{(2)}\mathbf{f}^{(0)}(0) + \mathbf{a}^{(3)}\mathbf{g}^{(0)}(0),$$
$$\mathbf{g}^{(2)} = \mathbf{b}^{(1)}\mathbf{f}^{(1)}(0) + \mathbf{b}^{(2)}\mathbf{g}^{(1)}(0) + \mathbf{b}^{(3)}\mathbf{f}^{(0)}(0) + \mathbf{b}^{(4)}\mathbf{g}^{(0)}(0).$$

Thus, the computed displacements and transverse stresses are

$$u_1 = \epsilon(q_3^+ - q_3^-)\frac{C + Dz}{a^2}x_1\left(\frac{x_1^2}{a^2} + \frac{x_2^2}{b^2} - 1\right) - \epsilon^3(q_3^+ - q_3^-)d_6x_1,$$
$$u_2 = \epsilon(q_3^+ - q_3^-)\frac{C + Dz}{b^2}x_2\left(\frac{x_1^2}{a^2} + \frac{x_2^2}{b^2} - 1\right) - \epsilon^3(q_3^+ - q_3^-)d_7x_2,$$

$$u_3 = -\frac{1}{4}(q_3^+ - q_3^-)D\left(\frac{x_1^2}{a^2} + \frac{x_2^2}{b^2} - 1\right)^2 - \epsilon^2(q_3^+ - q_3^-)$$
$$\times\left[(3d_2 + d_3)\frac{x_1^2}{a^2} + (d_2 + 3d_3)\frac{x_2^2}{b^2} - d_2 - d_3\right] \quad (30)$$
$$+ \epsilon^4[-q_3^+ d_1 + (q_3^+ - q_3^-)(c_3 d_1 + d_9)],$$

$$\sigma_{13} = -\epsilon^2(q_3^+ - q_3^-)d_4 x_1,$$
$$\sigma_{23} = -\epsilon^2(q_3^+ - q_3^-)d_5 x_2, \quad (31)$$
$$\sigma_{33} = \epsilon^3[-q_3^+ + (q_3^+ - q_3^-)(c_3 + d_8)],$$

where

$$d_1 = Q\frac{1}{\lambda + 2\mu}, \quad d_2 = \frac{1}{a^2}Q\frac{\lambda}{\lambda + 2\mu}(C + Dz),$$
$$d_3 = \frac{1}{b^2}Q\frac{\lambda}{\lambda + 2\mu}(C + Dz),$$
$$d_4 = \frac{2}{a^2}\left(\frac{3}{a^2} + \frac{1}{b^2}\right)(Q - \bar{Q})\gamma(C + Dz), \quad (32)$$
$$d_5 = \frac{2}{b^2}\left(\frac{1}{a^2} + \frac{3}{b^2}\right)(Q - \bar{Q})\gamma(C + Dz),$$
$$d_6 = Q\left(\frac{d_4}{\mu} - \frac{6d_2 + 2d_3}{a^2}\right), \quad d_7 = Q\left(\frac{d_5}{\mu} - \frac{6d_3 + 2d_2}{b^2}\right),$$
$$d_8 = Q(d_4 + d_5), \quad d_9 = Q\frac{\lambda(d_6 + d_7) + d_8}{\lambda + 2\mu}.$$

The longitudinal stresses obtained from Eq. (5) are

$$\sigma_{11} = \epsilon(q_3^+ - q_3^-)(C + Dz)\left[\frac{\gamma}{a^2}\left(\frac{3x_1^2}{a^2} + \frac{x_2^2}{b^2} - 1\right)\right.$$
$$\left. + \frac{\gamma - 2\mu}{b^2}\left(\frac{x_1^2}{a^2} + \frac{3x_2^2}{b^2} - 1\right)\right] - \epsilon^3\left\{q_3^+\frac{\lambda}{\lambda + 2\mu}\right.$$
$$\left. + (q_3^+ - q_3^-)\left[\gamma d_6 + (\gamma - 2\mu)d_7 - \frac{\lambda}{\lambda + 2\mu}(c_3 + d_8)\right]\right\},$$
$$\sigma_{22} = \epsilon(q_3^+ - q_3^-)(C + Dz)\left[\frac{\gamma - 2\mu}{a^2}\left(\frac{3x_1^2}{a^2} + \frac{x_2^2}{b^2} - 1\right)\right.$$
$$\left. + \frac{\gamma}{b^2}\left(\frac{x_1^2}{a^2} + \frac{3x_2^2}{b^2} - 1\right)\right]$$
$$- \epsilon^3\left\{q_3^+\frac{\lambda}{\lambda + 2\mu} + (q_3^+ - q_3^-)\left[\gamma d_7 + (\gamma - 2\mu)d_6\right.\right.$$
$$\left.\left. - \frac{\lambda}{\lambda + 2\mu}(c_3 + d_8)\right]\right\},$$
$$\sigma_{12} = \epsilon(q_3^+ - q_3^-)\frac{4\mu}{a^2 b^2}(C + Dz)x_1 x_2. \quad (33)$$

Note that $d_1$–$d_9$ can be evaluated by straightforward quadratures. For a homogeneous plate, the in-plane displacements $u_1$ and $u_2$ are polynomials of degree 3 in $x_3$, and the transverse shear stresses $\sigma_{13}$ and $\sigma_{23}$ are polynomials of degree 2. The orders of in-plane displacements and transverse shear stresses agree with those presumed in the third-order plate theory [7]. This is, however, not the case for a functionally graded plate whose material moduli vary in the thickness direction. Therefore, results predicted by the higher-order, classical and first-order plate theories may not be satisfactory. Note that in the latter two theories, a linear distribution of the in-plane displacements is assumed. This establishes the necessity of using a 3D formulation such as the present one to calculate deformations of a functionally graded plate.

## 5. Numerical results

A functionally graded material is made by mixing two distinct material phases, for example, a metal and a ceramic. The locally effective material properties are evaluated by the Mori–Tanaka scheme [8,9]. It should be noted that in general there is no representative volume element to be defined in functionally gradient materials, the average field estimates can only be applied with a reasonable degree of confidence [10].

Consider a two-phase composite consisting of a matrix phase denoted by subscript 1 and a particulate phase denoted by the subscript 2, respectively. The composite is reinforced by spherical particles, randomly distributed in the plate plane. The locally effective bulk modulus $K$ and shear modulus $\mu$ of the functionally gradient material are given

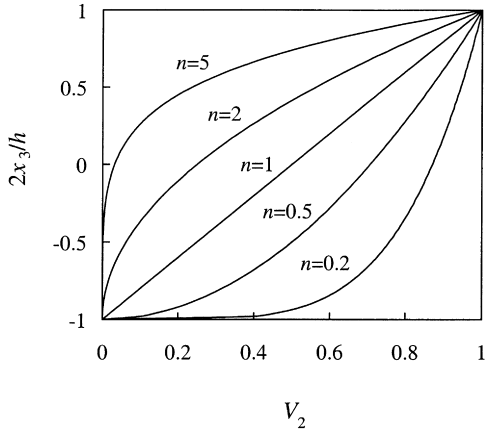


Fig. 2. Through-the-thickness distribution of the volume fraction of the ceramic phase in the functionally graded plate.

by the Mori–Tanaka estimates [8,9] as

$$\frac{K-K_1}{K_2-K_1}=V_2\Big/\left(1+(1-V_2)\frac{K_2-K_1}{K_1+(4/3)\mu_1}\right),$$

$$\frac{\mu-\mu_1}{\mu_2-\mu_1}=V_2\Big/\left(1+(1-V_2)\frac{\mu_2-\mu_1}{\mu_1+f_1}\right), \tag{34}$$

$$f_1=\frac{\mu_1(9K_1+8\mu_1)}{6(K_1+2\mu_1)}.$$

The locally effective heat conductivity coefficient $\kappa$ is given by [11]

$$\frac{\kappa-\kappa_1}{\kappa_2-\kappa_1}=\frac{V_2}{1+(1-V_2)((\kappa_2-\kappa_1)/3\kappa_1)}. \tag{35}$$

The coefficient of thermal expansion $\alpha$ is determined in terms of the correspondence relation [12]

$$\frac{\alpha-\alpha_1}{\alpha_2-\alpha_1}=\left(\frac{1}{K}-\frac{1}{K_1}\right)\Big/\left(\frac{1}{K_2}-\frac{1}{K_1}\right). \tag{36}$$

Here $V_2$ is the volume fraction of the particulate phase. The Mori–Tanaka estimates on statistically homogeneous composites with spherical reinforcements coincide with the Hashin–Shtrikman upper and lower bounds on elastic moduli [13], when the stiffer phase serves as a matrix or reinforcement of well-ordered composites, respectively.

In the following numerical results, the metal is taken as the matrix phase and the ceramic is taken as the particulate phase. We assume that the volume fraction of the ceramic phase is given by

$$V_2=\left(\frac{h+2x_3}{2h}\right)^n. \tag{37}$$

Fig. 2 shows the through-thickness variation of the volume fraction of the ceramic for $n=0.2, 0.5, 1, 2, 5$. Note that the volume fraction of the metal is high near the bottom surface of the plate, and that of ceramic high near the top surface.

In actual service conditions, zirconia top coat is typically employed as a thermal barrier on Ni-based structural components in aircraft engines. The constituent materials of the functionally graded plate are taken to be nickel-based alloy, Monel (70Ni–30Cu), and zirconia with material properties [14–16]

$$\begin{aligned}
&K_m=227.24\ \text{GPa},\quad \mu_m=65.55\ \text{GPa},\\
&\alpha_m=15\times10^{-6}/\text{K},\quad \kappa_m=25\ \text{W/mK},\ \text{for Monel},\\
&K_c=125.83\ \text{GPa},\quad \mu_c=58.077\ \text{GPa},\\
&\alpha_c=10\times10^{-6}/\text{K},\quad \kappa_c=2.09\ \text{W/mK},\ \text{for zirconia}.
\end{aligned} \tag{38}$$

In the linear theory used here, results for complex loadings can be obtained by superposing results for each of the simple loading. We assume that $T^-=q_3^-=0$ on the bottom surface of the elliptic plate. Two simple loading conditions, namely a uniform temperature change and a uniform normal pressure on the top surface are examined in the following numerical examples. The physical quantities are non-dimensionalized by

$$\bar{T}=\frac{T(x_3)}{T^+},\quad \bar{u}_3=\frac{u_3(x_3)}{5h\alpha^*T^+},\quad \bar{\sigma}_{11}=\frac{\sigma_{11}(x_3)}{E^*\alpha^*T^+}, \tag{39}$$

for the applied temperature load $T^+$, and by

$$\begin{aligned}
&\bar{u}_1=\frac{E^*u_1(-a,0,x_3)}{q_3^+a},\quad \bar{u}_3=\frac{E^*u_3(0,0,x_3)}{q_3^+a},\\
&\bar{\sigma}_{11}=\frac{\sigma_{11}(0,0,x_3)}{q_3^+},\quad \bar{\sigma}_{13}=\frac{\sigma_{13}(-a,0,x_3)}{q_3^+},\\
&\bar{\sigma}_{33}=\frac{\sigma_{33}(-a,0,x_3)}{q_3^+},
\end{aligned} \tag{40}$$

for the applied mechanical pressure $-q_3^+$, where $E^*=1$ GPa and $\alpha^*=10^{-6}$/K. The span-to-thickness ratio $2a/h$ is taken as 10.

Figs. 3–5 depict the through-thickness distributions of the dimensionless temperature $\bar{T}$, deflection $\bar{u}_3$ and longitudinal stress $\bar{\sigma}_{11}$ in the plate under the uniform thermal load $T^+$. Note that these quantities only vary in the thickness direction, i.e. they are uniform in a plane parallel to the reference plane $x_3=0$. Moreover, results due to the thermal load are valid for a plate of arbitrary shape. The through-thickness variation of the temperature in a homogeneous ceramic plate, which coincides with that in a homogeneous metallic plate, is linear and the temperature at a point in a homogeneous plate is always greater than that at the corresponding point in a functionally graded (FG) metal–ceramic plate with $n=0.2$, 0.5, 1, 2 or 5. The deflection of a point in the upper half of the plate is upward and that of a point in the lower half of the plate is downward. Except for the FG plate with $n=5$ whose deflections are intermediate between those of a ceramic plate and a metallic plate, the magnitude of the deflection of a point in the FG plate with $n=0.2$, 0.5, 1 or 2 is smaller than that of the corresponding point in the ceramic plate. Of course, because of the lower

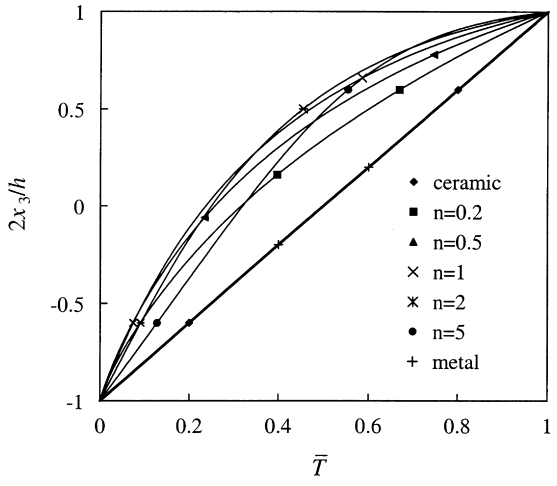


Fig. 3. Through-the-thickness distribution of the dimensionless temperature field $\bar{T}$ in the functionally graded plate under the thermal load.

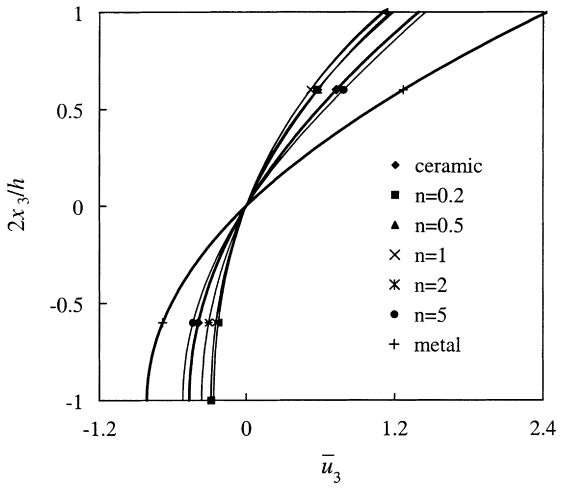


Fig. 4. Through-the-thickness distribution of the dimensionless deflection $\bar{u}_3$ of the functionally graded plate under the thermal load.

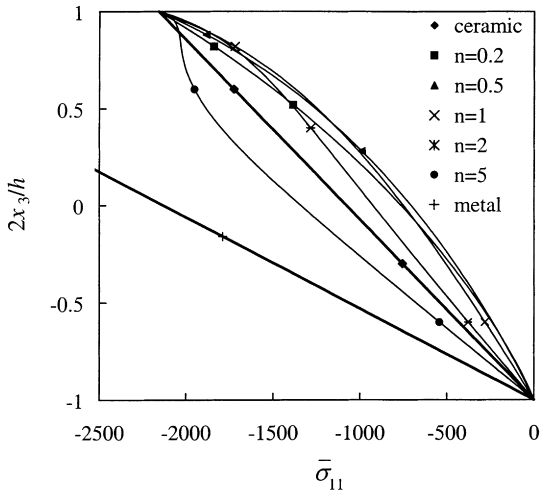


Fig. 5. Through-the-thickness distribution of the dimensionless longitudinal stress $\bar{\sigma}_{11}$ of the functionally graded plate under the thermal load.

value of the coefficient of thermal expansion, the magnitude of the deflection of a point in the ceramic plate is less than that of the corresponding point in the metallic plate. As exhibited in Fig. 5, the longitudinal stress, $\bar{\sigma}_{11}$, is compressive throughout the plate, and the maximum compressive stress occurs at a point on the top surface and minimum value of zero at a point on the bottom surface of the FG plate. Except at points on the top and bottom surfaces, the magnitude of the compressive stresses at a point in an FG plate with $n = 0.2$, 0.5, 1 or 2 is less than that at the corresponding point in either the ceramic or the metallic plate.

In Figs. 6–10 we have plotted the through-thickness variations of the displacements $\bar{u}_1$ and $\bar{u}_3$, and stresses $\bar{\sigma}_{11}$, $\bar{\sigma}_{13}$ and $\bar{\sigma}_{33}$ for (a) a circular plate (i.e. $a/b = 1$), (b) an elliptic plate with $a/b = 0.5$, and (c) an infinite strip (i.e. $a/b = 0$) whose top surface is loaded by the uniform mechanical pressure $-q_3^+$. The volume fraction of the FG plate is taken as $n = 0.5$ or 2 in these figures. It is clear that the through-thickness distributions of these quantities are similar for the three values of $a/b$, however, the magnitudes at the corresponding points are different. The transverse normal stress, $\bar{\sigma}_{33}$, does not depend upon the ratio $a/b$. Markers for different values of $n$ have been omitted in Figs. 6, 9 and 10 because the value at a point in an FG plate is very close to that at the corresponding point in a homogeneous metallic or ceramic plate.

The values of the in-plane displacement $\bar{u}_1$ (cf. Fig. 6) and the lateral deflection $\bar{u}_3$ (cf. Fig. 7) at a point of the FG plate with $n = 0.5$ or 2 lie between those at the corresponding points of the metallic and ceramic plates. The deflection is nearly constant through the thickness of the plate; this trend agrees with the assumption of constant deflection made in various plate theories. The tensile and compressive values of the longitudinal stress, $\bar{\sigma}_{11}$ (cf. Fig. 8), are maximum at a point on the top and bottom surfaces of the FG plate, respectively. For $n = 0.5$ and 2, the maximum value of the transverse shear stress, $\bar{\sigma}_{13}$ (cf. Fig. 9), occurs at a point a little below the mid-plane of the plate, and its magnitude is close to that in a metallic or a ceramic plate. The through-thickness distribution of $\bar{\sigma}_{13}$ is nearly parabolic for $a/b = 0$, 0.5 and 1. The magnitude of the transverse normal stress, $\bar{\sigma}_{33}$ (cf. Fig. 10), at any point in an FG plate is very close to that at the corresponding point in a homogeneous plate. In the absence of any interlayer in an FG plate, the out-of-plane stresses $\sigma_{13}$, $\sigma_{23}$ and $\sigma_{33}$ are not important and are negligible as compared to the longitudinal stress $\sigma_{11}$.

## 6. Conclusions

We have analyzed thermomechanical deformations of a linear elastic functionally graded elliptic plate with rigidly clamped edges. Because of the assumption of linearity, deformations due to thermal and mechanical loads applied to the top and bottom surfaces of the plate are separately computed. Deformations due to the temperature varying only in the thickness direction are calculated analytically, and those due to the mechanical load are obtained by the method of asymptotic expansion. It is found that the assumption of constant deflection usually made in plate theories is not valid for the case of the thermal load, but it is a good approximation for the mechanical load. The cubic through-thickness distribution of the in-plane displacements and the quadratic through-thickness distribution of transverse shear stresses assumed in the higher-order plate theory [7] agree with the present solution only for a homogeneous plate. However, this is not the case for a functionally graded plate whose deformations depend on the volume fraction of the constituent materials. The gradients in material properties significantly affect the response of a functionally graded plate under thermal loads. The deflection and the longitudinal stress at a point in a functionally graded elliptic plate are not necessarily between those at the corresponding

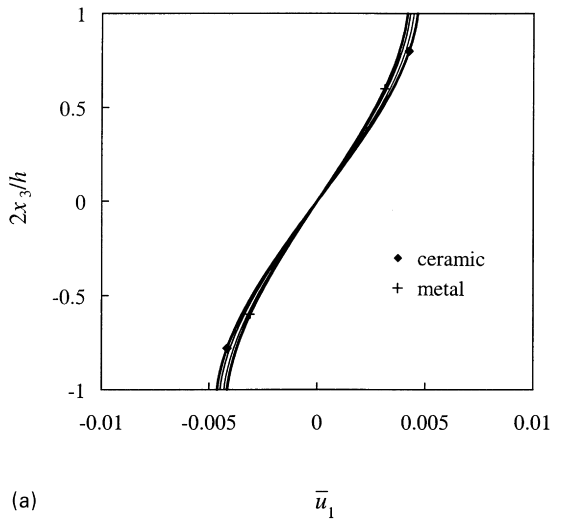


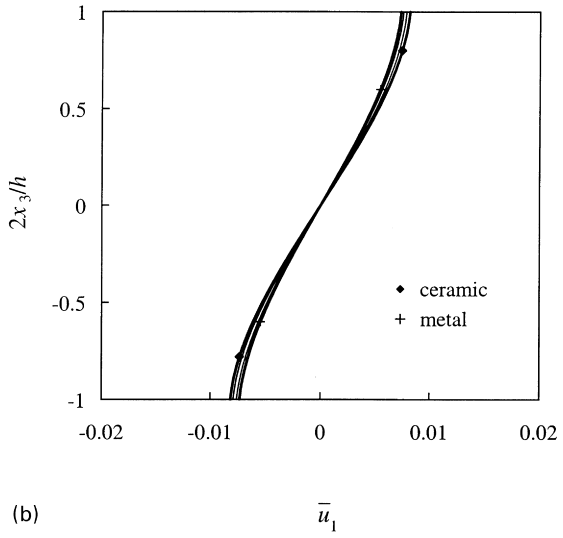


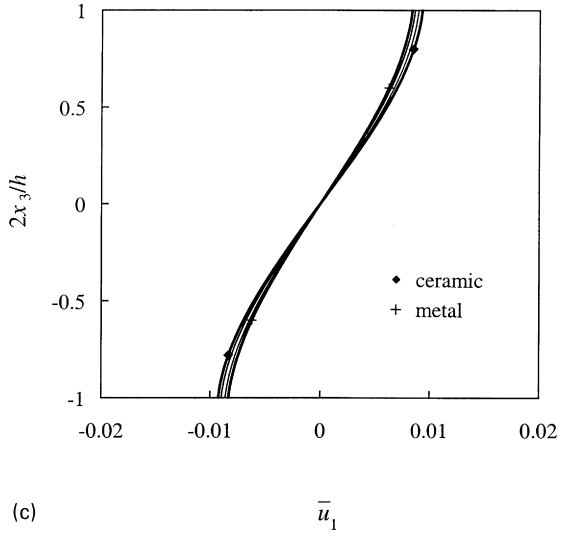


Fig. 6. Through-the-thickness distribution of the dimensionless in-plane displacement $\bar{u}_1$ of (a) a circular plate ($a/b = 1$), (b) an elliptic plate ($a/b = 0.5$), and (c) an infinite strip ($a/b = 0$), under the mechanical load.

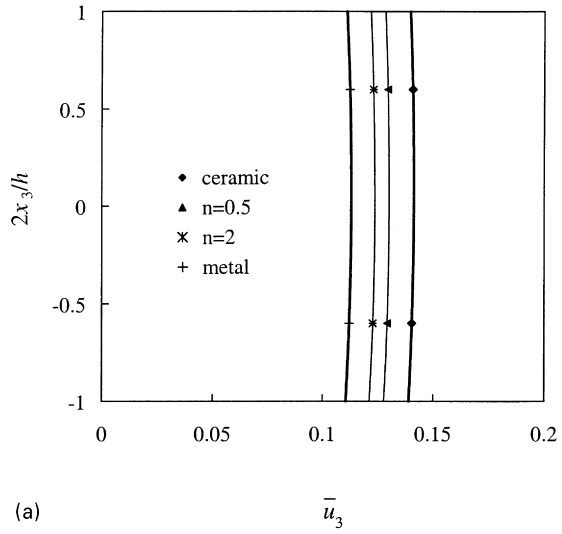


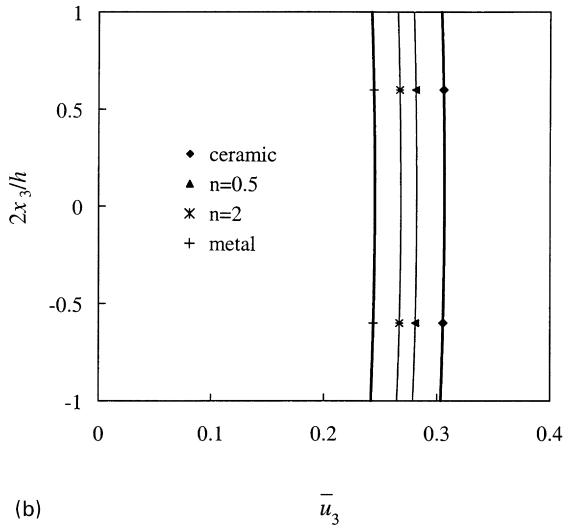


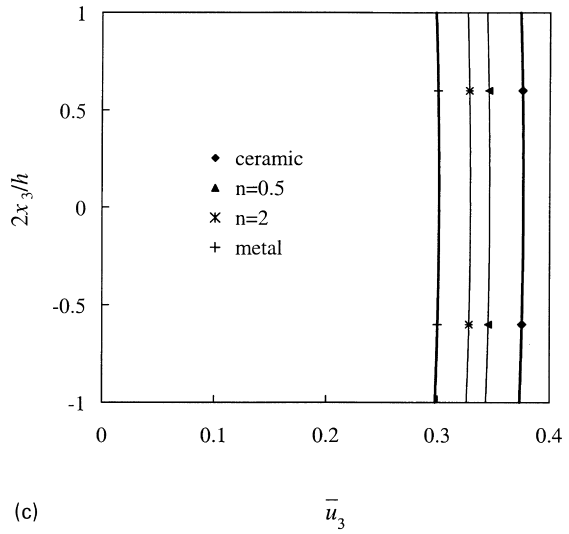


Fig. 7. Through-the-thickness distribution of the dimensionless deflection $\bar{u}_3$ of (a) a circular plate ($a/b = 1$), (b) an elliptic plate ($a/b = 0.5$), and (c) an infinite strip ($a/b = 0$), under the mechanical load.

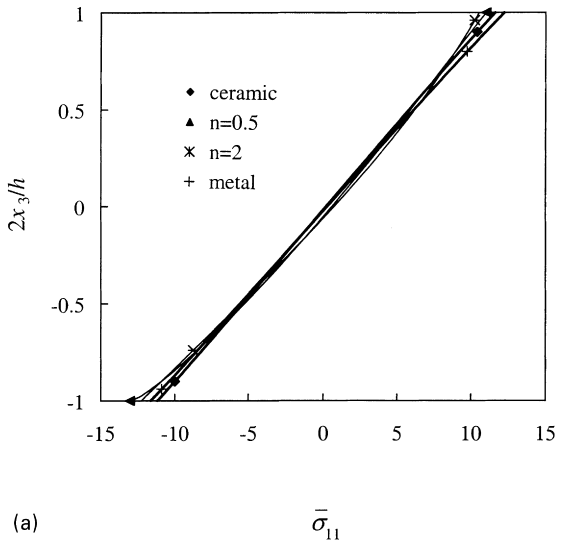


(a)

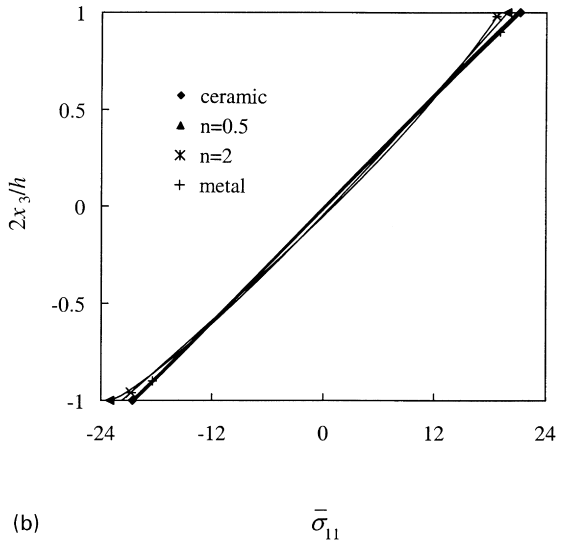


(b)

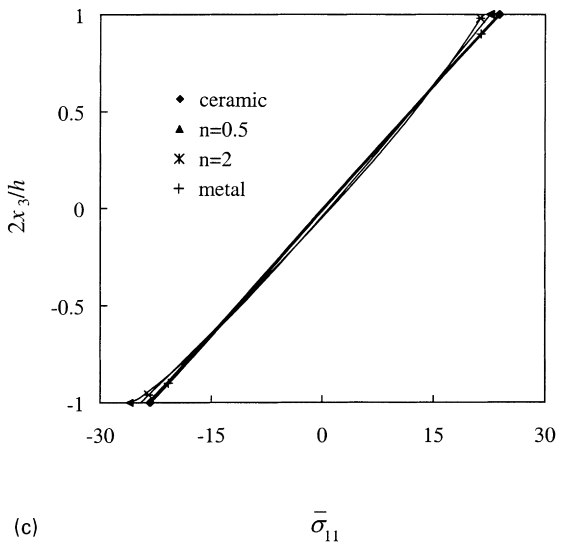


(c)

Fig. 8. Through-the-thickness distribution of the dimensionless longitudinal stress $\bar{\sigma}_{11}$ of (a) a circular plate ($a/b = 1$), (b) an elliptic plate ($a/b = 0.5$), and (c) an infinite strip ($a/b = 0$), under the mechanical load.

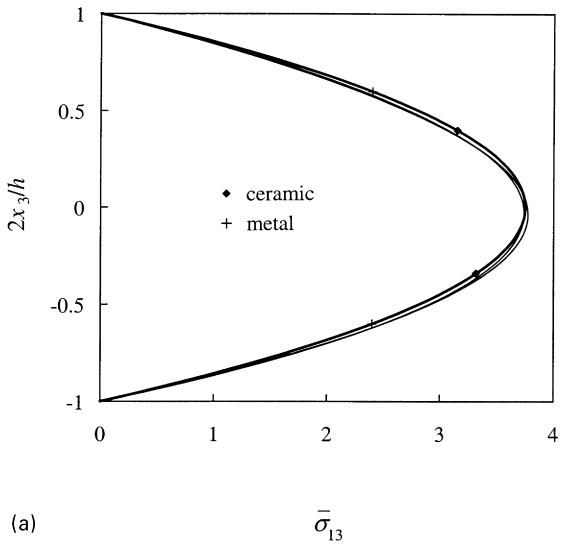


(a)

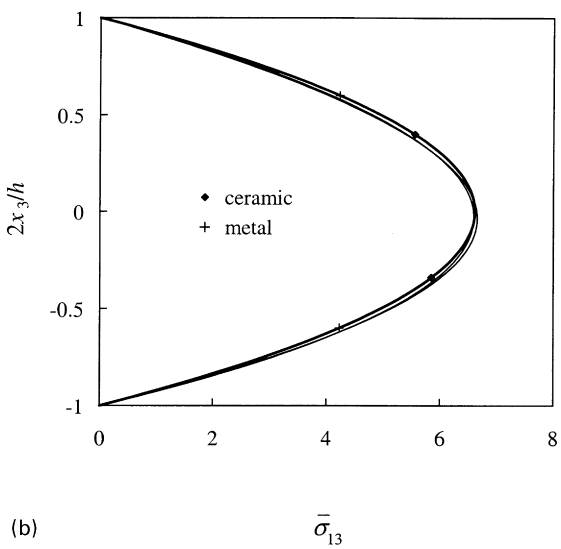


(b)

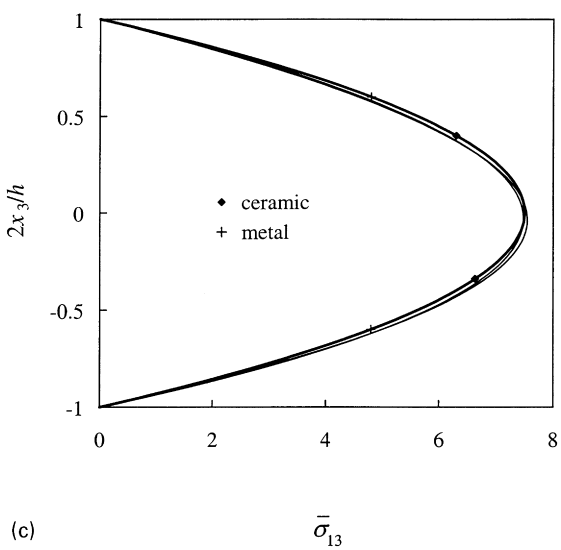


(c)

Fig. 9. Through-the-thickness distribution of the dimensionless transverse shear stress $\bar{\sigma}_{13}$ of (a) a circular plate ($a/b = 1$), (b) an elliptic plate ($a/b = 0.5$), and (c) an infinite strip ($a/b = 0$), under the mechanical load.

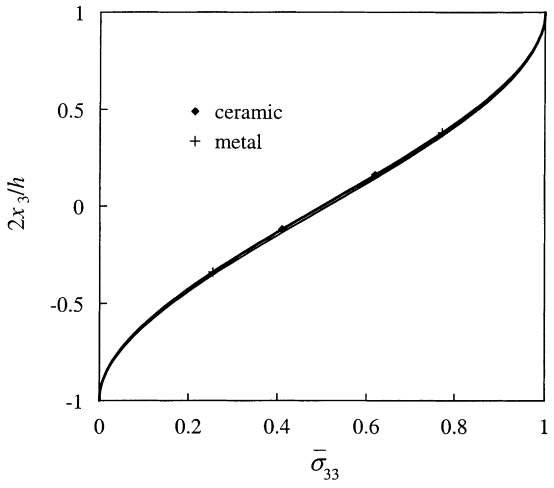


Fig. 10. Through-the-thickness distribution of the dimensionless transverse normal stress $\bar{\sigma}_{33}$ of an elliptic plate for an arbitrary value of *a*/*b*, under the mechanical load.

points in identical homogeneous metallic and ceramic plates.

## References

[1] Reddy JN. Mechanics of laminated composite plates: theory and analysis. Boca Raton, FL: CRC Press, 1997.
[2] Aboudi J. Mechanics of composite materials—a unified micromechanical approach. Amsterdam: Elsevier, 1991.
[3] Reddy JN, Chin CD. Thermomechanical analysis of functionally graded cylinders and plates. J Thermal Stresses 1998;21:593–626.
[4] Rogers TG, Watson P, Spencer AJM. An exact three-dimensional solution for normal loading of inhomogeneous and laminated anisotropic elastic plates of moderate thickness. Proc R Soc London Ser A 1992;437:199–213.
[5] Wang YM, Tarn JQ. A three-dimensional analysis of anisotropic inhomogeneous and laminated plates. Int J Solids Struct 1994;31:497–515.
[6] Tarn JQ, Wang YM. Asymptotic thermoelastic analysis of anisotropic inhomogeneous and laminated plates. J Thermal Stresses 1995;18:35–58.
[7] Reddy JN. A simple higher-order theory for laminated composite plates. J Appl Mech 1984;51:745–52.
[8] Mori T, Tanaka K. Average stress in matrix and average elastic energy of materials with misfitting inclusions. Acta Metall 1973;21:571–4.
[9] Benveniste Y. A new approach to the application of Mori–Tanaka's theory in composite materials. Mech Mater 1987;6:147–57.
[10] Reiter T, Dvorak GJ, Tvergaard V. Micromechanical models for graded composite materials. J Mech Phys Solids 1997;45:1281–302.
[11] Hatta H, Taya M. Effective thermal conductivity of a misoriented short fiber composite. J Appl Phys 1985;58:2478–86.
[12] Rosen BW, Hashin Z. Effective thermal expansion coefficients and specific heats of composite materials. Int J Engng Sci 1970;8:157–73.
[13] Hashin Z, Shtrikman S. A variational approach to the theory of the elastic behavior of multiphase materials. J Mech Phys Solids 1963;13:213–22.
[14] Murphy G. Properties of engineering materials. 3rd ed. Scranton, PA: International Textbook Company, 1957.
[15] Van Vlack LH. Elements of materials science and engineering. 5th ed. Reading, MA: Addison-Wesley, 1985.
[16] Praveen GN, Reddy JN. Nonlinear transient thermoelastic analysis of functionally graded ceramic–metal plates. Int J Solids Struct 1998;35:4457–76.